


# Magnetic and electrical transport properties in GdAlSi and SmAlGe

Jing Gong(巩静), Huan Wang(王欢), Xiao-Ping Ma(马小平), Xiang-Yu Zeng(曾祥雨), Jun-Fa Lin(林浚发), Kun Han(韩坤), Yi-Ting Wang(王乙婷), and Tian-Long Xia(夏天龙)

**Citation:**Chin. Phys. B, 2024, 33 (**7**): 077302. DOI: 10.1088/1674-1056/ad41ba
Journal homepage: http://cpb.iphy.ac.cn; http://iopscience.iop.org/cpb

**What follows is a list of articles you may be interested in**

---

## Recent progress on valley polarization and valley-polarized topological states in two-dimensional materials

Fei Wang(王斐), Yaling Zhang(张亚玲), Wenjia Yang(杨文佳), Huisheng Zhang(张会生), and Xiaohong Xu(许小红)
Chin. Phys. B, 2024, 33 (**1**): 017306. DOI: 10.1088/1674-1056/ad0713

## Electrically controllable spin filtering in zigzag phosphorene nanoribbon based normal—antiferromagnet—normal junctions

Ruigang Li(李锐岗), Jun-Feng Liu(刘军丰), and Jun Wang(汪军)
Chin. Phys. B, 2024, 33 (**1**): 017304. DOI: 10.1088/1674-1056/acf82a

## Electric modulation of anisotropic magnetoresistance in Pt/$HfO_{2-x}$/$NiO_y$/Ni heterojunctions

Xiaoyu Ye(叶晓羽), Xiaojian Zhu(朱小健), Huali Yang(杨华礼), Jipeng Duan(段吉鹏), Cui Sun(孙翠), and Run-Wei Li(李润伟)
Chin. Phys. B, 2023, 32 (**8**): 087305. DOI: 10.1088/1674-1056/acd2b6

## Controllable synthesis of ultrathin vanadium oxide nanobelts via an EDTA-mediated hydrothermal process

Yu-Xiang Qin(秦玉香), Cheng Liu(刘成), Wei-Wei Xie(谢威威), Meng-Yang Cui(崔梦阳)
Chin. Phys. B, 2016, 25 (**2**): 027307. DOI: 10.1088/1674-1056/25/2/027307

## Post-annealing effect on the structural and mechanical properties of multiphase zirconia films deposited by a plasma focus device

I. A. Khan, R. S. Rawat, R. Ahmad, M. A. K. Shahid
Chin. Phys. B, 2013, 22 (**12**): 127306. DOI: 10.1088/1674-1056/22/12/127306

---

# Magnetic and electrical transport properties in GdAlSi and SmAlGe

Jing Gong(巩静)[1,2], Huan Wang(王欢)[1,2], Xiao-Ping Ma(马小平)[1,2], Xiang-Yu Zeng(曾祥雨)[1,2], Jun-Fa Lin(林浚发)[1,2], Kun Han(韩坤)[1,2], Yi-Ting Wang(王乙婷)[1,2], and Tian-Long Xia(夏天龙)[1,2,3,4,†]

[1] *Department of Physics, Renmin University of China, Beijing* 100872, *China*
[2] *Beijing Key Laboratory of Opto-electronic Functional Materials & Micro-nano Devices, Renmin University of China, Beijing* 100872, *China*
[3] *Key Laboratory of Quantum State Construction and Manipulation (Ministry of Education), Renmin University of China, Beijing* 100872, *China*
[4] *Laboratory for Neutron Scattering, Renmin University of China, Beijing* 100872, *China*

(Received 20 March 2024; revised manuscript received 16 April 2024; accepted manuscript online 23 April 2024)

We conduct a detailed examination of the magnetic and electrical transport properties in GdAlSi and SmAlGe crystals, which possess a LaPtSi-type structure (space group $I4_1md$). The magnetic susceptibility data unambiguously reveal magnetic ordering below a characteristic transition temperature ($T_N$). For GdAlSi, a hysteresis loop is observed in the magnetization and magnetoresistance curves within the *ab* plane when the magnetic field is applied below $T_N$, which is around 32 K. Notable specific heat anomalies are detected at 32 K for GdAlSi and 6 K for SmAlGe, confirming the occurrence of magnetic transitions. In addition, the extracted magnetic entropy at high temperatures is consistent with the theoretical value of $R\ln(2J+1)$ for $J = 7/2$ in $Gd^{3+}$ and $J = 5/2$ in $Sm^{3+}$, respectively. SmAlGe also exhibits Schottky-like specific heat contributions. Additionally, both GdAlSi and SmAlGe exhibit positive magnetoresistance and a normal Hall effect.

**Keywords:** crystal growth, magnetism, magnetotransport properties, specific heat

**PACS:** 73.43.Qt, 75.47.–m, 75.60.Ej, 81.10.Fq **DOI:** 10.1088/1674-1056/ad41ba

## 1. Introduction

Recently, the fascinating interplay between electronic correlations and topology has ignited considerable interest in magnetic Weyl semimetals.[1–5] The *Ln*Al*X* (*Ln* = rare earth, *X* = Si, Ge) family offers an excellent platform for investigating their distinctive topological characteristics and rich magnetic properties, which is exemplified by the discovery of pressure-induced superconductivity and a spin Hall effect in LaAl*X*,[6,7] the observation of anisotropic anomalous Hall effects and a topological magnetic phase in CeAl*X*,[8–12] the measurement of a significant anomalous Hall conductivity and a field-induced Lifshitz transition in PrAl*X*,[13–17] and the detection of quantum oscillations, an anomalous Nernst effect, and the formation of helical incommensurate spin density waves in NdAl*X*.[18–22]

The insights from earlier research suggest that replacing the rare earth elements in the LnAl*X* series can lead to a spectrum of magnetic and transport characteristics. This variability spurs our interest in examining the properties of SmAl*X* and GdAl*X*. To date, SmAlSi has displayed Shubnikov–de Haas oscillations, topological spiral magnetism, and a Kramers nodal line.[23–27] However, there is a lack of research on the magnetic and electrical transport properties of SmAlGe single crystals. These discoveries solidify our intention to delve deeper into SmAlGe. Concerning GdAl*X*, GdAlGe exists in a tetragonal phase at temperatures above 1300 K, whereas the orthorhombic phase is formed below this threshold.[28–30] This contrasts with the tetragonal LnAl*X* family, complicating direct comparisons of their physical properties. To date, only a couple of studies have been published on the tetragonal GdAlSi single crystal,[31,32] highlighting the importance of a more thorough examination of its electronic and magnetic properties.

In this work, we have successfully grown single crystals of GdAlSi and SmAlGe using the flux method and have conducted a thorough investigation of their magnetic and electrical transport properties. Analysis of powder x-ray diffraction (XRD) patterns from crushed samples confirms that both GdAlSi and SmAlGe crystallize in a noncentrosymmetric structure with the space group $I4_1md$. We observe magnetic order below temperatures of 32 K and 6 K for GdAlSi and SmAlGe, respectively. For GdAlSi, we detect a field-induced phase transition with a loop both in magnetization and magnetoresistance (MR) curves. A positive MR, attributed to the Lorentz force, is observed in both GdAlSi and SmAlGe. Furthermore, by analyzing the normal Hall effect, we estimate the carrier concentrations to be approximately $\sim 1.1 \times 10^{21}$ cm$^{-3}$ at 2 K for GdAlSi and $\sim 2.5 \times 10^{21}$ cm$^{-3}$ for SmAlGe. The maximum mobility up to 96 cm$^2\cdot$V$^{-1}\cdot$s$^{-1}$ and 50 cm$^2\cdot$V$^{-1}\cdot$s$^{-1}$ for GdAlSi and SmAlGe are obtained.

†Corresponding author. E-mail: tlxia@ruc.edu.cn

© 2024 Chinese Physical Society and IOP Publishing Ltd 

## 2. Experiment

Single crystals of GdAlSi and SmAlGe were grown by the self-flux method. The Gd/Sm ingot, Al column, Si powder and Ge pieces were combined in ratios of Gd : Al : Si = 1 : 10 : 1 and Sm : Al : Ge = 1 : 10 : 1, then placed into an corundum crucible and vacuum sealed in a quartz tube. The quartz tube was placed in a box furnace, which is heated to 1150 ℃ at a rate of 60 ℃/h, and held for two hours. Then, it was cooled to 750 ℃ with a rate of 3 ℃/h, at which the excess Al flux was separated from the crystals by centrifugation. The atomic proportions of GdAlSi and SmAlGe were verified to be Gd : Al : Si = 1 : 1 : 1 and Sm : Al : Ge = 1 : 1 : 1, respectively, using energy dispersive x-ray spectroscopy (EDS, Oxford X-Max 50). The single crystal and powder x-ray diffraction (XRD) data for GdAlSi and SmAlGe were collected from a Bruker D8 Advance x-ray diffractometer using Cu $K_\alpha$ radiation. The refinement of the data was performed using TOPAS-4.2 software. An atomic-resolution high-angle annular dark field (HAADF) image was obtained with a spherical-aberration corrected JEOL ARM200F instrument equipped with double-aberration correctors and operated at 200 kV. The magnetic properties of the samples were measured with a Quantum Design magnetic property measurement system (QD MPMS-3). The electrical resistivity, specific heat, and Hall effect were measured in another Quantum Design physical property measurement system (QD PPMS-14T). Resistivity, magnetoresistance, and Hall resistivity measurement were performed by the four-probe method. To eliminate the influence from voltage probe misalignment, the raw resistivity data were evaluated by the formulae: $\rho_{xx}(B) = [\rho_{xx}(-9\,\mathrm{T} \rightarrow 9\,\mathrm{T}) + \rho_{xx}(9\,\mathrm{T} \rightarrow -9\,\mathrm{T})]/2$ and $\rho_{xy}(B) = [\rho_{xy}(-9\,\mathrm{T} \rightarrow 9\,\mathrm{T}) - \rho_{xy}(9\,\mathrm{T} \rightarrow -9\,\mathrm{T})]/2$.

## 3. Results and discussion

### 3.1. Crystal structure

As shown in Fig. 1(a), the structure consists of stacks of Gd/Sm, Al, and Si/Ge layers along the $c$-axis. The single-crystal XRD patterns for GdAlSi and SmAlGe, as shown in the upper panels of Figs. 1(c) and 1(d), respectively, reveal the surface of the samples with the (00$l$) plane, which is presented in the insets of Figs. 1(c) and 1(d). The powder XRD patterns for GdAlSi and SmAlGe are displayed in the lower panels of Figs. 1(c) and 1(d), respectively, which show no trace of any other impurity phase. From previous reports on LnAl$X$ family, it is now clear that LnAl$X$ family belongs to the noncentrosymmetric space group $I4_1md$ (No. 109).[8,10,15,20,22,26,31] Subsequently, a refinement of the powder XRD pattern was performed using the space group $I4_1md$. The obtained lattice parameters for GdAlSi are $a = b = 4.1278$ Å, $c = 14.4323$ Å, and for SmAlGe, they are $a = b = 4.1957$ Å, $c = 14.5880$ Å. Table 1 summarizes the refinement parameters for GdAlSi and SmAlGe. The crystal structure of as-grown GdAlSi was further confirmed by the transmission electron microscopy (TEM) data. Figure 1(b) shows an atomically resolved high-angle annular dark-field (HAADF) image of GdAlSi recorded along the [001] zone axis with the corresponding fast Fourier transform (FFT) images inserted. A simulation of the model structure is overlaid with an enlarged image from Fig. 1(b) as shown in the upper-right inset, where Gd, Al, and Si atoms are represented as purple, white, and blue balls, respectively. The lower-right inset presents a typical selected-area electron diffraction (SAED) pattern taken along the [001] zone axis. The diffraction spots can be well indexed with respect to the space group $I4_1md$, with $a = b = 4.08$ Å, which is consistent with the result obtained from XRD measurement.

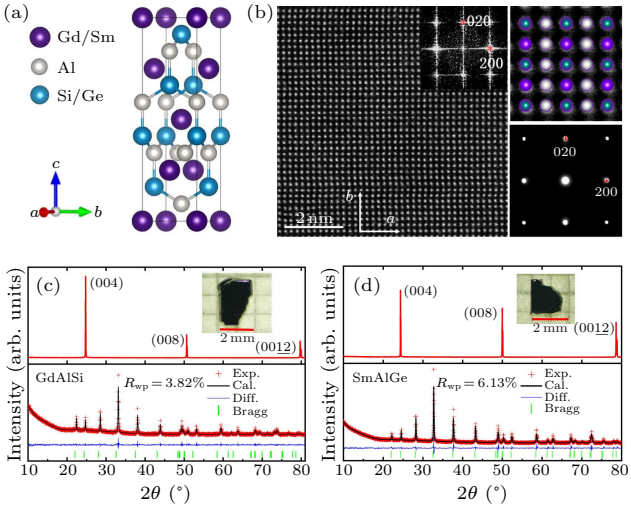



**Fig. 1.** (a) Crystal structure of non-centrosymmetric GdAlSi and SmAlGe with space group $I4_1md$ (No. 109). (b) An atomically resolved high-angle annular dark-field (HAADF) image of GdAlSi recorded along the [001] zone axis. Inset: fast Fourier transformation (FFT) of HAADF image. Upper right panel: a simulation of the model structure is overlaid with an enlarged image. Lower right panel: the FFT of SAED in GdAlSi. [(c), (d)] Upper: single crystal XRD pattern of the (00$l$) plane. Inset: picture of the polished crystal. Lower: the x-ray powder-diffraction pattern of GdAlSi and SmAlGe. The values of $R_{wp}$ for GdAlSi and SmAlGe are 3.82% and 6.13%, respectively.

**Table 1.** Structure parameters of GdAlSi and SmAlGe.

| Compound | GdAlSi | SmAlGe |
|---|---|---|
| Space group | $I4_1md$ (No. 109) | |
| Crystal structure | LaPtSi-type | |
| $a$ (Å) | 4.1278 | 4.1957 |
| $c$ (Å) | 14.4323 | 14.5880 |
| $V$ (Å$^3$) | 245.9081 | 256.8057 |
| $R_{wp}$ (%) | 3.82 | 6.13 |

### 3.2. Resistivity and specific heat

Figures 2(a) and 2(b) show the temperature dependence of longitudinal resistivity ($\rho_{xx}$) for GdAlSi and SmAlGe, respectively, which indicates typical metallic behavior. It can be seen that the resistivity shows a kink at 32 K for GdAlSi, indicating the Néel temperature, and this is also evidenced in the specific heat [Fig. 2(c)]. The magnetic phase transition

temperature is consistent with previous reports.[31,32] In general, a kink or drop on resistivity curve may happen related to transitions. However, in the magnetic SmAlGe, the interaction between the electrons and spin may be too weak and no kink or drop is observed at $T_N$ in the resistivity. Similar behavior has also been reported in $MnSb_6Te_{10}$[33] and $Eu_3In_2P_4$,[34] etc.

The measurement of specific heat is a valuable technique for investigating magnetic ordering phenomena in materials. It not only indicates the magnetic ordering temperature but can also be employed to estimate the magnetic entropy, which, in turn, can provide information about crystalline electric field (CEF). The specific heat of GdAlSi and SmAlGe, as well as their nonmagnetic isostructural LaAlSi and LaAlGe, in zero magnetic field is presented in Figs. 2(c) and 2(d). As the temperature decreases, a peak emerge around 32 K for GdAlSi and 6 K for SmAlGe, indicating the emergence of magnetic phase transition. In contrast, the specific heat of LaAlSi and LaAlGe exhibits no anomalies, which is consistent with that expected for nonmagnetic reference compounds.

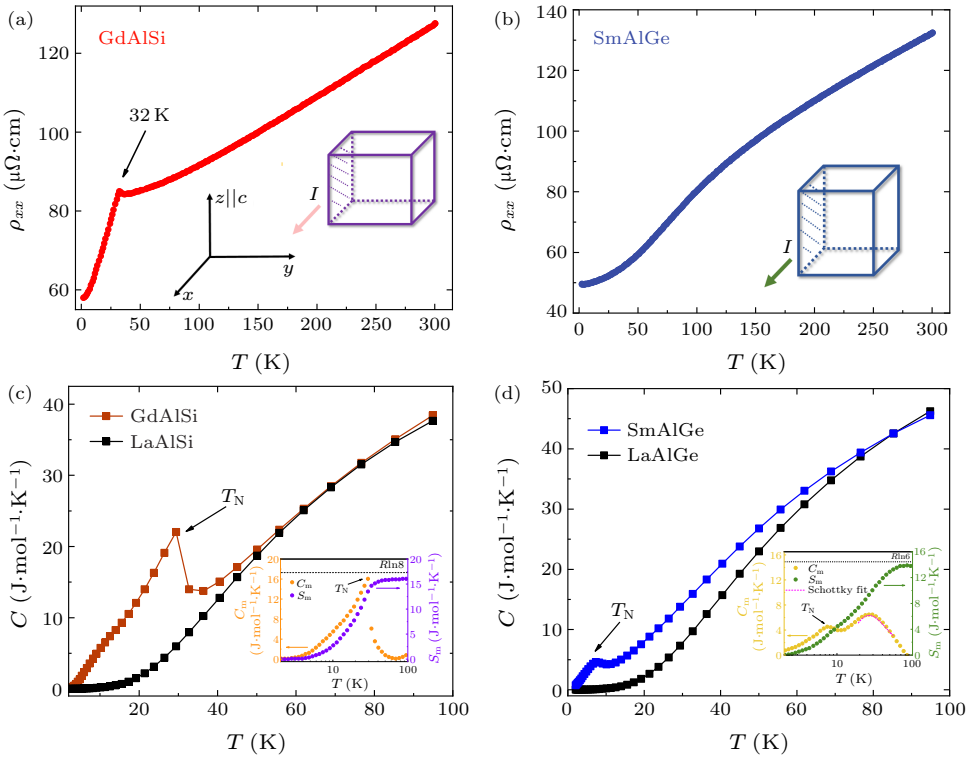



**Fig. 2.** [(a), (b)] Temperature dependence of the resistivity $\rho_{xx}$ for GdAlSi and SmAlGe, respectively. The inset illustrates the definition of a Cartesian coordinate system based on the tetragonal lattice. [(c), (d)] Temperature dependence of the specific heat in GdAlSi and SmAlGe. Inset: magnetic specific heat $C_m$ and magnetic entropy $S_m$ of GdAlSi and SmAlGe. The carmine dashed line is the Schottky fits of SmAlGe. The two horizontal black dashed lines stand for $R\ln 8$ and $R\ln 6$, respectively.

The magnetic contribution of GdAlSi and SmAlGe to specific heat $C_m$ are calculated by subtracting the data of isostructural non-magnetic LaAlSi and LaAlGe $C_{La}$, as shown in the inset of Figs. 2(c) and 2(d). The sharp peaks observed around 32 K in GdAlSi and 6 K in SmAlGe are indicative of magnetic phase transitions. Figure 2(d) shows a broad peak around 26 K, which is related to the Schottky anomaly contributed by the CEF splitting of $Sm^{3+}$ atomic levels. This behavior of the specific heat has also been observed in CeAlSi,[8] NdAlSi,[18,22] and SmAlSi.[26] The Schottky specific heat $C_{sh}$ of two levels is estimated using the equation[35]

$$C_{sh} = nR\left(\frac{\Delta}{T}\right)^2\left(\frac{g_0}{g_1}\right)\frac{e^{\Delta/T}}{\left[1+\left(\frac{g_0}{g_1}\right)e^{\Delta/T}\right]^2}, \quad (1)$$

where $n$ is the number of Sm atom in one formula, $R$ is the gas constant, $\Delta$ is the energy separation between the lowest and first excited states measured in K, and $g_0/g_1$ is the degeneracy ratio between the ground state and the excited state. For SmAlGe, the parameters used are $n = 1$ and $g_0/g_1 = 1/2$, respectively. The Schottky fits (carmine dashed line) yield a CEF gap $\Delta = 6.1$ meV in SmAlGe. Because the $Gd^{3+}$ ion has a zero orbital magnetic moment ($L = 0$),[36–38] the crystal field splitting is negligible, resulting in no Schokkty anomaly observed in GdAlSi. To examine the energy spectrum of the CEF states, the magnetic entropy $S_m(T)$ is calculated according to the equation

$$S_m(T) = \int_0^T \frac{C_m(T)}{T}\,dT, \quad (2)$$

and plotted in the insets of Figs. 2(c) and 2(d). The magnetic entropy saturates around 100 K at value of 16 J·mol$^{-1}$·K$^{-1}$ and 14 J·mol$^{-1}$·K$^{-1}$ for GdAlSi and SmAlGe, which is close

to $R\ln(2J+1) = R\ln 8$ and $R\ln 6$ expect for $J(\mathrm{Gd}^{3+}) = 7/2$ and $J(\mathrm{Sm}^{3+}) = 5/2$, respectively.

### 3.3. Magnetic properties

Figures 3(a) and 3(c) show the temperature-dependent magnetic susceptibilities $\chi(T)$ with $H \parallel c$ and $H \parallel ab$ under the zero-field-cooled (ZFC) and field-cooled (FC) modes for GdAlSi and SmAlGe, respectively. With $H \parallel ab$, the ZFC and FC curves show a kink at 32 K in GdAlSi, which marks the onset of magnetic order. As the temperature further decreases, the ZFC and FC curves do not saturate, as shown in the inset of Fig. 3(a). With $H \parallel c$, ZFC and FC nearly saturate at low temperature with slight bifurcation. As we measured $\chi(T)$ at 50 Oe, it differs from the previously reported results at 1000 Oe.[31] For SmAlGe, with $H \parallel ab$, as the temperature decreases, the ZFC and FC curves bifurcate and begin to drop at 6 K, which marks the onset of magnetic order as shown in the inset of Fig. 3(c). With $H \parallel c$, the ZFC and FC curves slightly bifurcate around 6 K and do not saturate at 2 K.

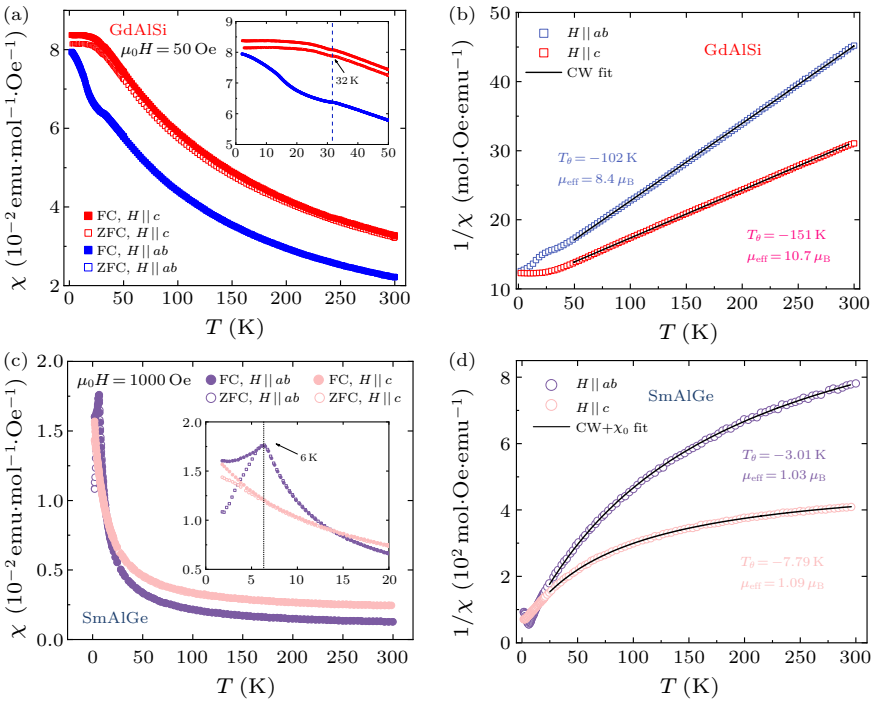



**Fig. 3.** [(a), (c)] Low temperature dependence of the magnetic susceptibility $\chi(T)$ of GdAlSi and SmAlGe. Inset shows an enlarged view of the magnetic susceptibility. [(b), (d)] Temperature dependence inverse magnetization of GdAlSi from 50 K to 300 K and SmAlGe from 25 K to 300 K.

Figure 3(b) shows the inverse magnetic susceptibility $1/\chi$ curve fitted by the Curie–Weiss law expression between 50 K to 300 K for GdAlSi,

$$\chi(T) = \frac{C}{T-\theta}, \tag{3}$$

where $C$ is the Curie constant, and $\theta$ is the Weiss temperature. From the fitting of Eq. (3), $\theta^{ab} = -102$ K and $\theta^{c} = -151$ K are obtained, which indicates the dominant AFM interaction for GdAlSi. The $C$ is 8.9 emu·K·mol$^{-1}$·Oe$^{-1}$ ($H \parallel ab$) and 14.4 emu·K·mol$^{-1}$·Oe$^{-1}$ ($H \parallel c$). The effective magnetic moments along different directions are estimated with relation $\mu_{\rm eff} = \sqrt{8C}$. The yielding effective magnetic moment is 8.4 $\mu_{\rm B}$ with $H \parallel ab$, which approaches to the theoretical value of a free $Gd^{3+}$ ion, which is approximately 7.9 $\mu_{\rm B}$. With $H \parallel c$, the effective moment is determined to be 10.7 $\mu_{\rm B}$, which is larger than the theoretical value of a free $Gd^{3+}$ ion. The surplus moment may be attributed to the conduction electron spin polarization.[39–42]

A significant curvature of inverse magnetic susceptibility ($1/\chi$) occurs in SmAlGe [Fig. 3(d)], which is usually observed in metallic rare earth magnets due to a large Pauli contribution to the susceptibility.[43] In this case, the curve can be described by a modified Curie–Weiss law within the temperature range of 25 K to 300 K,

$$\chi(T) = \chi_0 + \frac{C}{T-\theta}, \tag{4}$$

where $\chi_0$ is the temperature-independent term including the contribution from the core diamagnetism and the Van Vleck paramagnetism. From the fitting of Eq. (4), $\theta^{ab} = -3.01$ K and $\theta^{c} = -7.79$ K are obtained, which indicates the dominant AFM interaction in SmAlGe. The $C$ is 0.13 emu·K·mol$^{-1}$·Oe$^{-1}$ ($H \parallel ab$) and 0.15 emu·K·mol$^{-1}$·Oe$^{-1}$ ($H \parallel c$). The effective magnetic moment approaches 1.0 $\mu_{\rm B}$ both in the $ab$ plane and along the $c$-axis, which approaches the theoretical value of a free $Sm^{3+}$ ion ($\sim 0.85\ \mu_{\rm B}$). The parameters obtained from Eqs. (3) and (4) of the $\chi^{-1}(T)$ data are summarized in Table 2.

**Table 2.** The Curie constant $C$, the Weiss temperatures $\theta$ and the effective moments $\mu_{\rm eff} = \sqrt{8C}$ obtained from Curie–Weiss and modified Curie–Weiss fits to the high temperature $\chi(T)$ data for GdAlSi and SmAlGe.

| Compound | Field direction | $\chi_0$ | $C$ (emu·K·mol$^{-1}$·Oe$^{-1}$) | $\theta$ (K) | $\mu_{\rm eff}$ |
|---|---|---|---|---|---|
| GdAlSi | $H \parallel ab$ | – | 8.9 | −102 | 8.4 |
| | $H \parallel c$ | – | 14.4 | −151 | 10.7 |
| SmAlGe | $H \parallel ab$ | 0.00084 | 0.13 | −3.01 | 1.03 |
| | $H \parallel c$ | 0.00194 | 0.15 | −7.79 | 1.09 |

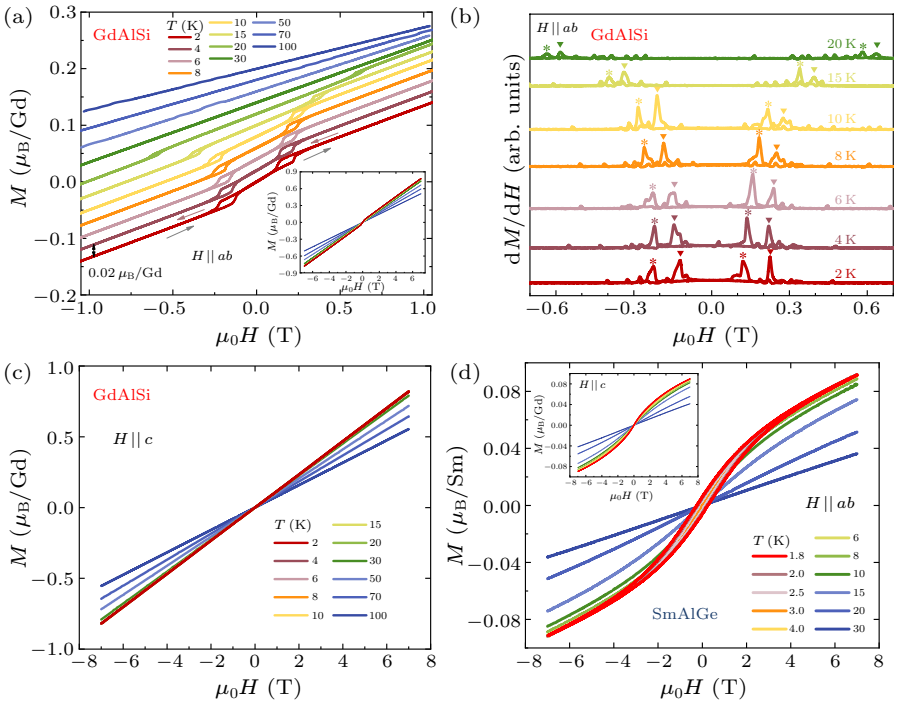



**Fig. 4.** (a) Field-dependent magnetization $M(H)$ of GdAlSi at different temperatures for $H \parallel ab$. The 2 K curve has correct values in units of 0.02 $\mu_{\rm B}$/Gd and the rest of the curves are shifted uniformly to improve visibility. Inset shows $M(H)$ measure up to a higher field of 7 T. (b) The derivatives of the $M$ ($H \parallel ab$) curves reveal four peaks. The triangular symbol and star symbol indicate the acsending field and descending field, respectively. (c) Field dependent magnetization $M(H)$ of GdAlSi at different temperatures for $H \parallel c$. (d) Field dependence of the $ab$ plane magnetic moment in SmAlGe. Inset: Isotherm $M(H)$ curves for $H \parallel c$.

Isothermal $M(H)$ curves with $H$ applied parallel to the $ab$ plane and along the $c$-axis in GdAlSi are shown in Figs. 4(a) and 4(c). The magnetization curves are linear at high temperatures, which corresponds to the paramagnetic state. A hysteresis behavior in low field occurs to each $M(H)$ curve below $T_{\rm N}$, which may implies a field-induced phase transition.[6,24,26,44] With the temperature decreases, the hysteretic metamagnetic transition shifts to lower fields. The $\mathrm{d}M/\mathrm{d}H$ as a function of field is shown in Fig. 4(b). The magnetizations are discovered to keep increasing as field increases and do not reach saturation at 2 K. The maximum moment approximately 0.77 $\mu_{\rm B}$/Gd with $H \parallel ab$, as shown in the inset of Fig. 4(a). With $H \parallel c$, the magnetization does not show any signature of saturation up to a field of 7 T at 2 K, and attains a value of only 0.75 $\mu_{\rm B}$/Gd as shown in Fig. 4(c), which confirms the antiferromagnetic ordering of the Gd moments.

The magnetization of SmAlGe as a function of field at different temperatures with $H \parallel ab$ and $H \parallel c$ is shown in Fig. 4(d). The magnetization curves are linear at high temperatures above $T_{\rm N}$, which corresponds to the paramagnetic state. With the temperature decreasing, the moments with $H \parallel ab$ gradually increase and a small hysteresis loop appears around zero field, which corresponds to the bifurcation behavior of the $\chi$–$T$ curve. At 2 K, the magnetization exhibits a continuous increase until the field reached 7 T. The maximum moment of $\sim 0.09$ $\mu_{\rm B}$/Sm with $H \parallel ab$. With $H \parallel c$, the magnetization also does not show any signature of saturation up to a field of 7 T at 1.8 K and attains a value of only 0.09 $\mu_{\rm B}$/Sm, as shown in the inset of Fig. 4(d).

### 3.4. Magnetoresistance and Hall effect

To investigate magnetotransport of GdAlSi, the field dependent MR are measured with $H \parallel ab$ and $H \parallel c$, as shown in Figs. 5(a) and 5(c), in which the MR is defined as $[\rho_{xx}(\mu_0 H) - \rho_{xx}(0)]/\rho_{xx}(0)$. Positive MRs are observed with $H \parallel ab$ and $H \parallel c$, which is due to the scattering of the conduction electrons in cyclotron motion of the carriers influenced by Lorentz force in magnetic field.[45] With $H \parallel ab$, hysteresis loops are observed at finite fields below 30 K, possibly due to metamagnetic transitions.[44,46] With the temperature decreases, the hysteresis loop shifts to lower field. This behavior is consistent with the $M(H)$ curve. Meanwhile, we measured the angular

MR, with the field directed at various angles ($\theta$) with respect to the $c$-axis in the $yz$ plane at 2 K, as depicted in Fig. 5(b). The schematic diagrams of experimental setup are shown in the inset of Fig. 5(b). The MR values increase with the applied field and do not saturate until 14 T. Figure 5(e) exhibits the field dependence of $\rho_{xx}$ at 2 K (below $T_N \sim 6$ K) and 8 K (above $T_N \sim 6$ K) for SmAlGe. The measurement configuration is shown in the inset of Fig. 5(e).

The field dependence of Hall resistivity of GdAlSi and SmAlGe at various temperatures are measured, as shown in Figs. 5(c), 5(d), and 5(f). The positive sign of Hall coefficient indicates that the charge carriers are hole-type in both GdAlSi and SmAlGe. The insets of Figs. 5(d) and 5(f) show carrier concentrations $n$ and mobilities $\mu$ as a function of temperature. Using the one-band model, the carrier concentration is estimated to be $\sim 1.1 \times 10^{21}$ cm$^{-3}$ and $\sim 2.5 \times 10^{21}$ cm$^{-3}$ at 2 K for GdAlSi and SmAlGe, respectively. The carrier concentrations in the LnAlSi family of compounds are higher than those in other compounds within the same family.[13,18,23,24,31] The mobilities of GdAlSi and SmAlGe equals 96 cm$^2$·V$^{-1}$·s$^{-1}$ and 50 cm$^2$·V$^{-1}$·s$^{-1}$ using $\mu = 1/(en\rho_{(0T)})$ as shown in the insets of Figs. 5(d) and 5(f).

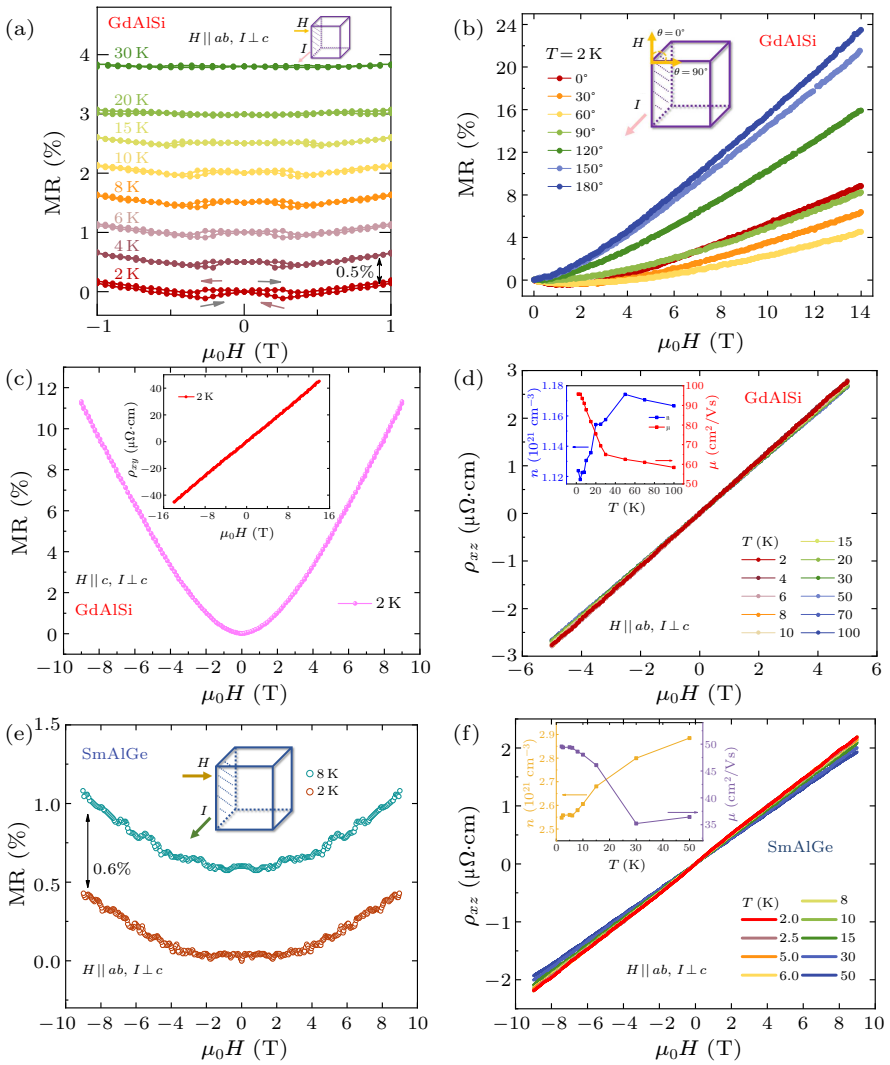



**Fig. 5.** (a) Magnetic field dependence of MR at various temperature measured with $H \parallel ab$ in GdAlSi. The 2 K curve has correct values in units of 0.5% and the rest of the curves are shifted uniformly to improve visibility. (b) The MR are shown at 2 K with the field pointing at several angles as indicated in the inset. (c) Magnetic field dependence of MR at 2 K with $H \parallel c$ in GdAlSi. Inset: field-dependent Hall resistivity curves for $H \parallel c$ at 2 K. (d) Field-dependent Hall resistivity curves for $H \parallel ab$ at different temperatures in GdAlSi. Inset: temperature dependence of $n$ and $\mu$. (e) MR curves of SmAlGe for $H \parallel ab$ at temperatures 2 K and 8 K. The 2 K curve has correct values in units of 0.6%, and the 8 K curve is shifted uniformly to improve visibility. (f) Field-dependent Hall resistivity curves for $H \parallel c$ at different temperatures in SmAlGe. Inset: temperature dependence of $n$ and $\mu$.

## 4. Conclusion

In summary, we have systematically investigated the magnetic and electrical transport properties of GdAlSi and SmAlGe, which have a LaPtSi-type structure (space group $I4_1md$). The magnetic phase transitions occur at 32 K for GdAlSi and at 6 K for SmAlGe, respectively. The results of the Curie–Weiss fitting indicate the presence of AFM interactions in both GdAlSi and SmAlGe. Additionally, GdAlSi

exhibits a field-induced phase transition in magnetization and MR. The normal Hall effect is observed in both GdAlSi and SmAlGe. The carrier concentration at 2 K is $\sim 1.1 \times 10^{21}$ cm$^{-3}$ and the mobility is 96 cm$^2\cdot$V$^{-1}\cdot$s$^{-1}$ for GdAlSi, while for SmAlGe, the carrier concentration is approximately $2.5 \times 10^{21}$ cm$^{-3}$ and the mobility is 50 cm$^2\cdot$V$^{-1}\cdot$s$^{-1}$. These findings not only provide a new platform for studying the transport properties of the *Ln*Al*X* (*Ln* = rare earth; *X* = Si, Ge) family but also deepen our understanding of the exotic physical phenomena associated with magnetic properties.

## Acknowledgments

J. Gong thanks Hao-yu Dong, Jian-feng Guo, and Fei-hao Pan for their fruitful discussions. This work was supported by the National Natural Science Foundation of China (Grant No. 12074425), the National Key R&D Program of China (Grant No. 2019YFA0308602), the Fundamental Research Funds for the Central Universities, and the Research Funds of Renmin University of China (Grant No. 23XNKJ22).

## References

[1] Fujishiro Y, Kanazawa N, Kurihara R, *et al.* 2021 *Nat. Commun.* **12** 317
[2] Yang H, Sun Y, Zhang Y, Shi W J, Parkin S S and Yan B 2017 *New J. Phys.* **19** 015008
[3] Yan B and Felser C 2017 *Annu. Rev. Conden. Matter Phys.* **8** 337
[4] Xu S Y, Belopolski I, Alidoust N, *et al.* 2015 *Science* **349** 613
[5] Lv B, Weng H, Fu B, *et al.* 2015 *Phys. Rev. X* **5** 031013
[6] Cao W, Zhao N, Pei C, *et al.* 2022 *Phys. Rev. B* **105** 174502
[7] Ng T, Luo Y, Yuan J, *et al.* 2021 *Phys. Rev. B* **104** 014412
[8] Yang H Y, Singh B, Gaudet J, *et al.* 2021 *Phys. Rev. B* **103** 115143
[9] Suzuki T, Savary L, Liu J P, Lynn J W, Balents L and Checkelsky J G 2019 *Science* **365** 377
[10] Hodovanets H, Eckberg C, Zavalij P, Kim H, Lin W C, Zic M, Campbell D, Higgins J and Paglione J 2018 *Phys. Rev. B* **98** 245132
[11] Puphal P, Pomjakushin V, Kanazawa N, *et al.* 2020 *Phys. Rev. Lett.* **124** 017202
[12] Piva M M, Souza J, Brousseau-Couture V, *et al.* 2023 *Phys. Rev. Res.* **5** 013068
[13] Lyu M, Xiang J, Mi Z, Zhao H, Wang Z, Liu E, Chen G, Ren Z, Li G and Sun P 2020 *Phys. Rev. B* **102** 085143
[14] Wu L, Chi S, Zuo H, Xu G, Zhao L, Luo Y and Zhu Z 2023 *npj Quantum Mater.* **8** 4
[15] Yang H Y, Singh B, Lu B, *et al.* 2020 *APL Mater.* **8** 011111
[16] Meng B, Wu H, Qiu Y, Wang C, Liu Y, Xia Z, Yuan S, Chang H and Tian Z 2019 *APL Mater.* **7** 051110
[17] Sanchez D S, Chang G, Belopolski I, *et al.* 2020 *Nat. Commun.* **11** 3356
[18] Wang J F, Dong Q X, Guo Z P, *et al.* 2022 *Phys. Rev. B* **105** 144435
[19] Wang J F, Dong Q x, Huang Y F, *et al.* 2022 arXiv:2201.06412 [cond-mat.mtrl-sci]
[20] Yang H Y, Gaudet J, Verma R, *et al.* 2023 *Phys. Rev. Mater.* **7** 034202
[21] Dong Q X, Wang J F, Zhang L B, *et al.* 2023 *Phys. Rev. B* **108** 205143
[22] Gaudet J, Yang H Y, Baidya S, *et al.* 2021 *Nat. Mater.* **20** 1650
[23] Cao W, Su Y, Wang Q, *et al.* 2022 *Chin. Phys. Lett.* **39** 047501
[24] Xu L, Niu H, Bai Y , *et al.* 2022 *J. Phys.: Condens. Matter.* **34** 485701
[25] Zhang Y, Gao Y, Gao X J, *et al.* 2023 *Commun. Phys.* **6** 134
[26] Yao X, Gaudet J, Verma R, Graf D E, Yang H Y, Bahrami F, Zhang R, Aczel A A, Subedi S, Torchinsky D H, *et al.* 2023 *Phys. Rev. X* **13** 011035
[27] Gao Y, Lei S, Clements E M, Zhang Y, Gao X J, Chi S, Law K T, Yi M, Lynn J W and Morosan E 2023 arXiv:2310.09364 [cond-mat.mtrl-sci]
[28] Pukas S, Lutsyshyn Y, Manyako M and Gladyshevskii E 2004 *J. Alloys Compd.* **367** 162
[29] Zhao J and Parthé E 1990 *Acta Crystall. Sec. C* **46** 2276
[30] Bobev S, Tobash P H, Fritsch V, Thompson J D, Hundley M F, Sarrao J L and Fisk Z 2005 *J. Solid State Chem.* **178** 2091
[31] Laha A, Kundu A K, Aryal N, *et al.* 2024 *Phys. Rev. B* **109** 035120
[32] Nag J, Das B, Bhowal S, Nishioka Y, Bandyopadhyay B, Kumar S, Kuroda K, Kimura A, Suresh K and Alam A 2023 arXiv:2312.11980 [cond-mat.str-el]
[33] Zhang X, Zhang S, Jiang Z, *et al.* 2021 arXiv:2111.04973 [cond-mat.mtrl-sci]
[34] Jiang J, Olmstead M M, Kauzlarich S M, Lee H O, Klavins P and Fisk Z 2005 *Inorg. Chem.* **44** 5322
[35] Gopal E 2012 *Specific heats at low temperatures* (Springer Science & Business Media)
[36] Bauer E and Rotter M 2010 *Properties and Applications of Complex Intermetallics* (World Scientific) p. 183
[37] Lüthi B 1976 *AIP Conf. Proc.* **34** 7
[38] Furrer A 2012 *Crystal field effects in metals and alloys* (Springer Science & Business Media)
[39] Wang C, Guo Y Q, Wang T and Yang S W 2020 *Chin. Phys. B* **29** 127502
[40] Burzo E, Urzu I and Pierre J 1972 *Phys. Status. Solidi. B* **51** 463
[41] Roeland L, Cock G, Muller F, Moleman A, McEwen K, Jordan R and Jones D 1975 *J. Phys. F: Met. Phys.* **5** L233
[42] Szade J and Less J 1987 *Common. Met.* **136** 101
[43] Mugiraneza S and Hallas A M 2022 *Commun. Phys.* **5** 95
[44] Shi M, Lei B, Zhu C, Ma D, Cui J, Sun Z, Ying J and Chen X 2019 *Phys. Rev. B* **100** 155144
[45] Pippard A B 1989 *Magnetoresistance in metals* (Cambridge University Press) **2**
[46] Tian S, Gao S, Nie S, *et al.* 2020 *Phys. Rev. B* **102** 035144